

# Rethinking failure in polymer networks: a probabilistic view on progressive damage

Noy Cohen<sup>a,b,\*</sup>, Nikolaos Bouklas<sup>b,c</sup>, and Chung-Yuen Hui<sup>b</sup>

<sup>a</sup>Department of Materials Science and Engineering, Technion - Israel Institute of Technology, Haifa 3200003, Israel

<sup>b</sup>Sibley School of Mechanical and Aerospace Engineering, Cornell University, Ithaca, New York 14853, USA

<sup>c</sup>Pasteur Labs, Brooklyn, NY 11205, USA

## Abstract

The mechanics of single-chain stretching and rupture are central to understanding the resilience of biological polymers and designing strong and tough soft materials such as double-network gels and multi-network elastomers. In this work, we develop a statistical mechanics based model that enables one to determine the distribution of forces along the chain segments. By combining the force distribution with a tilted bond potential that captures the stretch energy stored in these bonds, we calculate the corresponding activation energy required for bond dissociation. This allows us to determine the probability of bond (and consequently chain) failure. The proposed approach is simple, direct, and readily adaptable for constructing higher-level coarse-grained descriptions of damage and fracture in polymer networks. We demonstrated this by applying the theory to three problems of practical interest: (1) toughening via sacrificial bond rupture in polymer chains, (2) toughening of double network hydrogels, and (3) incorporation of the local chain model into a 3-dimensional constitutive relation that captures damage in elastomers. The latter was implemented through the micro-sphere framework, which accounts for different chain orientations, as well as the computationally inexpensive eight chain model. The findings from this work provide a physically-based model to quantify the stretching and failure of a single chain and pave the way to the integration of local damage models into 3-dimensional networks.

---

\*e-mail address: noyco@technion.ac.il

---

**Keywords:** Statistical mechanics; polymer networks; progressive damage and failure; chain scission; bond strength

# 1 Introduction

The stretching and rupture of individual polymer chains underpin modern multi-scale descriptions of damage, fracture, and adhesion in soft polymeric materials [1–6]. Constitutive models such as the three-, the four-, and the eight-chain network models [7–9] describe the nonlinear elasticity of rubbery networks comprising freely jointed chains (FJCs) [10, 11]. When chain rupture is incorporated, these models naturally extend to continuum descriptions of damage and Mullins-type softening [12, 13], readily providing a molecularly informed theory for adhesion models in elastomers [14–17].

Single-chain mechanics also appear explicitly in theories of fracture and adhesion. The classical Lake–Thomas (LT) theory relates the energy required to propagate a crack to the energy needed to rupture a single polymer chain between cross-link junctions, making chain-level failure the fundamental dissipative mechanism governing toughness [18]. This mechanism—energy dissipation through chain stretching and scission—has since been recognized as a central ingredient enabling the design of exceptionally tough soft materials such as double-network hydrogels [19] and multi-network elastomers [20], where controlled chain damage in sacrificial networks provides large distributed dissipation during crack growth. Recognizing that LT is a scaling law stemming from the idealization that rupture takes place on a single plane, recent works have also focused on the limitations of this assumption towards a more realistic resolution of damage zone size [21].

Many works developed models that account for rupture through probabilistic considerations [22–24], limiting values (in which failure is accounted for phenomenologically) [3, 25–27], and asymptotic approximations and matching [28–31]. Similar concepts guide models of protein-based networks [32–35] and adhesive failure, where debonding proceeds through sequential stretching and detachment of load-bearing chains or chain-like bridges [36, 37].

Recent advances in single-molecule force spectroscopy now allow direct measurement of

---

the energy stored in an individual polymer chain at rupture, enabling quantitative comparisons with the LT hypothesis that the chain-breaking energy equals the number of bonds in a chain times the C–C bond dissociation energy [38–40]. A recent analysis by Wang et al. [41] employed single-molecule force spectroscopy data to demonstrate that the stored energy per bond at the onset of fracture is approximately one-third of the dissociation energy of a C–C bond. Thus, the LT theory underestimates the fracture energy by about 60%. More advanced models for fracture have borrowed ideas from the phase field [42, 43] and gradient enhanced [44, 45] models, merging these with statistical mechanics theories [46–48].

In this contribution, statistical mechanics methodology is applied to better understand the origin of failure in chains. To this end, we derive a framework that approximates the distribution of forces and the consequent enthalpy of repeat units along a chain, an aspect that has been neglected in previous theories. We show that the forces are not distributed equally among chain segments, and the force is proportional to the orientation of a segment with respect to the end-to-end vector. By employing the tilted potential energy profile for the bonds along the chain [49, 50], we compute the activation energy required to dissociate a bond. This energy decreases as the chain stretches, and accordingly the probability of rupture increases. This approach is advantageous since it accounts for the stochastic nature of chain scission and inherently yields a maximum stretching force that can be exerted on the chain, above which bonds break spontaneously.

To demonstrate the predictive capability of the proposed theory, we apply it to three representative problems of practical interest. The first concerns chains with sacrificial bonds, in which sequential bond rupture governs energy dissipation and toughening. This is a common occurrence in biological polymers [50, 51]. The second addresses the overall mechanical behavior of double network hydrogels [52, 53], where a stiff sacrificial network and a soft stretchable network interact to drive strain localization. Notably, the characteristic stress-stretch curves of double network gels exhibit a softening “plateau” followed by strain-stiffening, which provide significant extensibility as compared to the standard elastomers. We adopt a non-affine model and adopt the model of Morovati et al. [54], which uses an intermediate network to model

the interaction between the two networks. As noted by Gong [53], this interaction is due to entanglement between broken fragments of stiff network with the soft network. The third application incorporates the chain model into a continuum network representation through (1) a micro-sphere-based integration [25, 55, 56] and (2) the eight chain model of Arruda and Boyce [9]. These frameworks are employed to study anisotropic damage accumulation under large deformations. This model can be naturally embedded into phase field and gradient damage frameworks, opening a new avenue for future studies of fracture in elastomers.

## 2 The free energy of a chain

Consider a FJC comprising  $n$  stretchable Kuhn segments with an initial (relaxed) length  $l_0$ . The chain is and its Kuhn segments stretch such that the end-to-end distance and direction are  $r$  and  $\hat{r}$ , respectively. We point out that one can either prescribe the stretching force  $f$  or the end-to-end distance  $r$  along the direction  $\hat{r}$ .

The number of conformations available to the chain under the end-to-end constraint is  $\Omega = n! / (\prod_i n^{(i)}!)$ , where  $n^{(i)}$  is the number of Kuhn segments that form an angle  $\theta^{(i)} \leq \theta \leq \theta^{(i)} + d\theta$  with the end-to-end vector  $\hat{r}$  [57, 58]. We denote the deformed length of the  $i$ -th segment by  $l^{(i)}$ .

The entropy of the chain is

$$S_c = k_b \ln(\Omega) \approx k_b \left( n \ln n - n - \sum_i (n^{(i)} \ln(n^{(i)}) - n^{(i)}) \right), \quad (1)$$

where Stirling's approximation is employed and  $k_b$  is the Boltzmann's constant. The chain is subjected to the constraints

$$n = \sum_i n^{(i)}, \quad (2)$$

$$r = \sum_i l^{(i)} n^{(i)} \cos \theta^{(i)}, \quad (3)$$

$$U_c = \sum_i n^{(i)} u^{(i)}, \quad (4)$$

where  $u^{(i)} = u(l^{(i)})$  is the potential energy of the  $i$ -th segment due to stretching and  $U_c$  is the total energy of the chain.

Following common practice [57, 58], we assume that the chain occupies the most probable conformation under the given constraints. This is equivalent to maximizing the entropy under the given constraints, i.e.

$$\tilde{S}_c(n^{(i)}, l^{(i)}, \alpha, \beta, \gamma) = S_c + k_b \left( \alpha \left( \sum_i n^{(i)} - n \right) + \frac{\beta}{l_0} \left( \sum_i l^{(i)} n^{(i)} \cos \theta^{(i)} - r \right) + \gamma \left( \sum_i n^{(i)} u^{(i)} - U_c \right) \right), \quad (5)$$

where  $\alpha$ ,  $\beta$ , and  $\gamma$  are Lagrange multipliers that enforce the constraints in Eqs. 2, 3, and 4. The maximization of Eq. 5 with respect to  $n^{(i)}$  and  $l^{(i)}$  yields

$$\frac{\partial \tilde{S}_c}{\partial n^{(i)}} = k_b \left( -\ln(n^{(i)}) + \alpha + \beta \frac{l^{(i)}}{l_0} \cos \theta^{(i)} + \gamma u^{(i)} \right) = 0, \quad (6)$$

and

$$\frac{\partial \tilde{S}_c}{\partial l^{(i)}} = k_b n^{(i)} \left( \frac{\beta}{l_0} \cos \theta^{(i)} + \gamma \frac{\partial u^{(i)}}{\partial l^{(i)}} \right) = 0, \quad (7)$$

respectively. From Eqs. 6 and 7, one can obtain

$$n^{(i)} = \exp(\alpha) \exp \left( \beta \frac{l^{(i)}}{l_0} \cos \theta^{(i)} + \gamma u^{(i)} \right), \quad (8)$$

and

$$\frac{\partial u^{(i)}}{\partial l^{(i)}} = -\frac{\beta}{l_0 \gamma} \cos \theta^{(i)}. \quad (9)$$

Note that as opposed to previous works [28, 29], the current formulation can also be used to determine the deformed length of a Kuhn segment corresponding to the maximum entropy configuration under prescribed boundary conditions.

Substituting Eq. 8 into the Eq. 1 yields the entropy

$$S_c = k_b \left( n \ln n - \alpha n - \frac{\beta}{l_0} r - \gamma U_c \right). \quad (10)$$

It remains to determine the Lagrange multipliers. The first law of thermodynamics reads

$dU_c = dW + TdS_c$ , where  $dW$  is an increment in the work done on the system. Accordingly, one can write

$$\frac{\partial U_c}{\partial U_c} = T \frac{\partial S_c}{\partial U_c} \Rightarrow \gamma = -\frac{1}{k_b T}. \quad (11)$$

Next, we employ Eq. 8 along with the constraint in Eq. 2 to write  $\exp \alpha = n/Z$ , where

$$Z = \int_0^\pi \exp \left( \beta \frac{l}{l_0} \cos \theta - \frac{u(l)}{k_b T} \right) d\Gamma, \quad (12)$$

is the partition function and  $d\Gamma = \sin \theta d\theta/2$  is the solid angle-based probability density function with  $0 \leq \theta \leq \pi$ . Note in Eq. 12 we convert the discrete summation to an integral and accordingly the deformed Kuhn length  $l = l(\theta, \beta(r))$ .

With Eqs. 8 and 12, we define the probability that a segment forms an angle  $\theta$  with  $\hat{r}$ ,

$$p_\theta(\theta, \beta(r)) = \frac{n^{(i)}}{n} = \frac{1}{Z} \exp \left( \beta \frac{l}{l_0} \cos \theta - \frac{u}{k_b T} \right), \quad (13)$$

such that  $\int_0^\pi p_\theta d\Gamma = 1$ . Using Eq. 13, Eq. 3 is

$$\rho = \frac{r}{nl_0} = \int_0^\pi \frac{l}{l_0} \cos \theta p_\theta(\theta, \beta(r)) d\Gamma, \quad (14)$$

where we define the ratio  $\rho$  between the end-to-end distance and the initial contour length of the chain and employ the relation  $n^{(i)} = np_\theta$ .

The force on the chain can be computed via (see derivation in Appendix A)

$$f = \frac{\partial W}{\partial r} = \frac{\partial (U_c - TS_c)}{\partial r} = \frac{k_b T}{l_0} \beta. \quad (15)$$

Before proceeding, we point out that the above framework recovers the classical FJC model in the case of inextensible bonds (i.e.  $u = 0$ ). The incorporation of an enthalpic term enables to capture the distribution of forces along the chain. Specifically, Eqs. 9 and 15 can be combined to give

$$\frac{\partial u}{\partial l} = f_b, \quad (16)$$

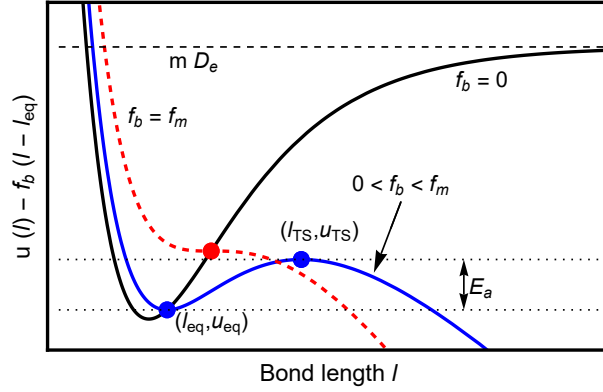


Figure 1: The potential energy landscape  $u(l) - f_b(l - l_{eq})$  as a function of the bond length  $l$ .

where  $f_b = f \cos \theta$  is the force on a Kuhn segment. This relation reveals that segments along the end-to-end vector experience different forces, with a maximum of  $f_b = f$  for segments that are aligned along  $\hat{\mathbf{r}}$  (i.e.  $\theta = 0$ ). Therefore, under a force  $f$ , the position of segments with  $\theta > 0$  are maintained mostly through entropic mechanisms that prevent their rotation.

To determine the response of the chains, the potential energy  $u$  of a Kuhn segment must be specified. Subsequently, we can prescribe (A) the end-to-end distance  $r$  or (B) the force  $f$  on the chain, and compute the corresponding  $\beta$  through the following procedures:

## 2.1 Procedure A

In the case of a prescribed  $r$ , Eq. 9 allows us to solve for the deformed lengths of the Kuhn segments along the chains as a function of  $\beta$  and  $\theta$ . Subsequently, one can plug this relation into Eq. 14 to numerically determine the  $\beta$ .

## 2.2 Procedure B

Alternatively, one can prescribe  $f$ , compute  $\beta = fl_0/(k_bT)$ , and then employ Eqs. 9 and 14 to determine the deformed length of the Kuhn segments and the end-to-end distance  $r$  (in this case,  $\beta$  is determined as a function of  $r$ ).

# 3 The energy of a repeat unit along the chain

Next we explore the enthalpic energy of the chain. Each Kuhn segment comprises  $m$  bonds (typically chemical C-C bonds) with an initial and a deformed length of  $l_0/m$  and  $l/m$ , respec-

tively. In the following, we assume that each bond follows the tilted Morse-based potential [40], and accordingly the total potential energy of a Kuhn segment is

$$u(l) = mD_e \left( 1 - \exp \left( -\frac{2f_m}{D_e} \left( \frac{l}{m} - \frac{l_0}{m} \right) \right) \right)^2. \quad (17)$$

Here,  $D_e$  is the dissociation energy, or the energy required to break a bond in the absence of an external force, and  $f_m \geq f_b$  is the maximum force that can be applied to a bond prior to breaking. Once an external force is applied (i.e.  $f_b > 0$ ), bonds stretch and alter the energy landscape. Through integration of Eq. 16, the potential energy can be written as  $u(l) - f_b(l - l_{eq})$ , where  $l_{eq}$  denotes the bond length at equilibrium. This energy generally has two extrema points - a minimum, corresponding to the equilibrium state in which the bond length is  $l = l_{eq}$ , and a maximum, which describes the transition state of a bond rupture event. Fig. 1 plots the potential energy landscape  $u(l) - f_b(l - l_{eq})$  as a function of the bond length  $l$  in the absence of a force (black curve), under an applied force  $0 < f_b < f_m$  (blue curve), and for  $f_b = f_m$  (red dashed curve).

The extrema under a force  $f_b$  can be determined from Eq. 16,

$$l = l_0 + \frac{mD_e}{2f_m} \ln \left( \frac{2(1 \pm \sqrt{1 - \tau})}{\tau} \right), \quad (18)$$

where the plus and the minus signs correspond to the transition state length  $l_{TS}$  and the equilibrium length  $l_{eq}$ , respectively, and we define the normalized force  $0 \leq \tau = f_b/f_m \leq 1$ . Note that in the limit  $f_b \rightarrow 0$ , the potential does not have a maximum and the equilibrium length  $l_{eq} = l_0$ . It is convenient to define the energies at the extrema points  $u_{TS} = u(l_{TS}) - f_b(l_{TS} - l_{eq})$  and  $u_{eq} = u(l_{eq})$ .

The rupture of a Kuhn segment depends on the activation energy (or energy barrier) between the equilibrium and the transition states [40]

$$E_a = u_{TS} - u_{eq} = mD_e \left( \sqrt{1 - \tau} + \frac{\tau}{2} \ln \left( \frac{1 - \sqrt{1 - \tau}}{1 + \sqrt{1 - \tau}} \right) \right), \quad (19)$$

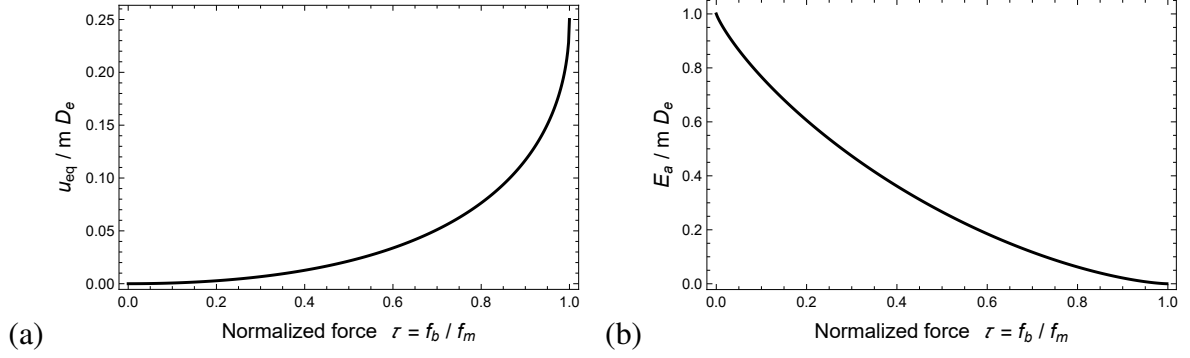


Figure 2: (a) The normalized equilibrium potential  $u_{eq}/mD_e$  and (b) the normalized activation energy  $E_a/mD_e$  as a function of the normalized force a bond experiences  $\tau = f_b/f_m$ .

where Eq. 18 is used. Specifically, for a given normalized force  $\tau$ , larger  $E_a$  corresponds to a low probability of a rupture, and once the maximum force is applied (i.e.  $f_b = f_m$ ),  $l_{TS} = l_{eq}$  the bond breaks spontaneously. Note that the activation energy  $E_a$  decreases monotonically, with the limiting values  $E_a = mD_e$  and  $E_a = 0$  for  $f_b \rightarrow 0$  and  $f_b = f_m$ , respectively. Figs. 2a and 2b plot the normalized equilibrium potential  $u_{eq}/mD_e$  and the activation energy  $E_a/mD_e$  as a function of  $\tau$ , respectively.

Chain scission occurs when one of the bonds in a Kuhn segment along the chain breaks. To capture the stochastic nature of chain failure, we define the probability to break a single bond along a Kuhn segment subjected to a normalized force  $\tau$  by

$$p_b(\tau) = \exp\left(-\frac{E_a(\tau)}{m k_b T}\right). \quad (20)$$

Note that  $0 < p_b \leq 1$ , with the limits  $p_b(E_a(\tau) \rightarrow \infty) \rightarrow 0$  and  $p_b(E_a(\tau) = 0) = 1$ . Therefore, the probability of chain rupture is

$$p_c(f) = 1 - p_{NR}, \quad (21)$$

where

$$\begin{aligned} p_{NR} &= \prod (1 - p_b(\tau)) \Rightarrow \ln p_{NR} = \sum \ln(1 - p_b(\tau)) \\ &\Rightarrow p_{NR} = \exp\left(\int_0^\pi \ln(1 - p_b(\tau)) d\Gamma\right), \end{aligned} \quad (22)$$

Table 1: Summary of model parameters.

Notation	Significance
$r$	End-to-end distance
$n$	Number of Kuhn segments in chain
$l_0, l$	initial, deformed length of Kuhn segment
$u$	Potential energy of Kuhn segment
$\rho = r/nl_0$	Ratio between $r$ and initial contour length of chain
$f, f_b$	Force on chain, Kuhn segment
$f_m$	Maximum force on Kuhn segment
$\tau = f_b/f_m$	Ratio between force on Kuhn segment and maximum force
$\beta$	Lagrange multiplier enforcing Eq. 3, determines the force on a chain
$D_e$	Dissociation energy required to break bond
$m$	Number of bonds in a Kuhn segment
$E_a$	Activation energy (energy barrier)
$p_b, p_c$	probability of breaking a bond, chain
$\boldsymbol{\sigma}, \mathbf{P}$	True (Cauchy), first Piola-Kirchhoff stress tensor

is the probability that none of the bonds break. In Eq. 22 the products and summations are carried over all Kuhn segments and we account for the distribution of forces along the chain, i.e. each Kuhn segment experiences the normalized force  $\tau$ . It is once again emphasized that the force experienced by the Kuhn segments depends on their orientation with respect to the end-to-end distance (recall  $\tau \sim \cos \theta$  through  $f_b$ ). Therefore,

$$p_c(f) = 1 - \exp \left( \int_0^\pi \ln(1 - p_b(\tau)) d\Gamma \right), \quad (23)$$

where  $p_b$  is given by Eq. 20.

For convenience, we summarize all of the model parameters in Table 1.

## 4 Mechanical response of single chains

### 4.1 The classical chain

To demonstrate the merit of the proposed framework, we consider a chain characterized by the maximum force  $f_m = 5 \text{ nN}$  and the Kuhn length  $l_0 = 1 \text{ nm}$ , where each Kuhn segment has  $m = 5$  chemical C-C bonds with  $D_e = 150 k_b T$  [39–41, 59]. The chain is stretched such that its end-to-end distance  $r$  increases from 0 to rupture.

Fig. 3a plots the normalized force on the chain  $f/f_m$  as a function of the normalized end-to-end distance  $\rho = r/nl_0$ . The force  $f$  is calculated via Eq. 15 through procedure A (Sec. 2.1) using the tilted Morse potential (Eq. 17). It is worth noting that Kuhn segments along the chain experience a force  $f_b \leq f$ , with  $f_b = f$  for segments that are aligned along the end-to-end vector (i.e  $\theta = 0$ ). The dotted and the dashed curves denote the predictions according to the FJC model with rigid Kuhn segments and the modified FJC (m-FJC), in which  $r/nl_0 = (\coth(f/f_c) - f_c/f)(1 + f/f_s)$  [39, 60]. The latter accounts for the entropic and enthalpic responses at low and high forces, with  $f_c \approx k_b T/l_0$  and  $f_s$  as the characteristic conformational and stretching tensions, respectively. In Fig. 3a, we follow experimental findings and set  $f_c \approx 4 \text{ pN}$  and  $f_s \approx 10 \text{ nN}$  and show that the present model follows the trend of the m-FJC. It is worth mentioning that the m-FJC overestimates the chain force and does not account for the limiting rupture force. The introduction of the tilted Morse potential in the proposed model includes a maximum force and therefore provides a practical physically-motivated tool to predict chain scission. The shaded region marks the forces for which the probability of failure is  $> 60\%$ .

To better understand the stochastic nature of chain scission, we examine the probability of chain scission for strong chemical bonds and weaker physical bonds. Typically, physical bonds are characterized by low dissociation energies ( $D_e \sim 1 - 50 k_b T$ ) and a maximum force of  $f_m \sim 10 - 100 \text{ pN}$  [35, 40, 61]. Fig. 3b plots the probability of rupture  $p_c$  (Eq. 23) as a function of the normalized chain force  $f/f_m$  for strong chemical ( $D_e = 150 k_b T$ ) and weak physical ( $D_e = 50 k_b T$ ) bonds. We find that the probability of failure for chains comprising strong chemical bonds with a high dissociation energy  $D_e$  is very small for  $f/f_m < 0.9$ , and

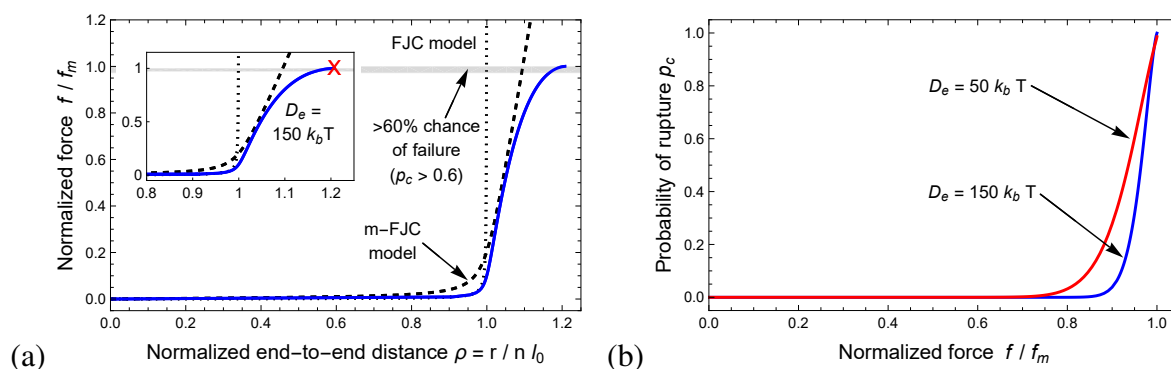


Figure 3: (a) The normalized force on the chain  $f/f_m$  as a function of the normalized end-to-end distance  $\rho = r/nl_0$ . (b) The probability of rupture  $p_c$  as a function of the normalized chain force  $f/f_m$ .

increases as forces near  $f_m$ . Weaker bonds have a higher probability of breaking at forces that are smaller relative to their corresponding maximum force  $f_m$ . This is particularly relevant for systems with sacrificial physical bonds, hidden length-type mechanisms, and mechanophore activation [20, 32, 35, 62]. Note that rupture is guaranteed ( $p_c = 1$ ) once the maximum force  $f = f_m$  is achieved.

## 4.2 A polymer chain with sacrificial bonds

Chains with sacrificial bonds are common in nature and synthetic systems [32, 35, 39, 63–65]. Typically, these bonds can be ionic bonds, hydrogen bonds, hydrophobic interactions, or Van der Waals [51, 66]. In the following, we employ our framework to investigate the influence of sacrificial bonds on two types of chain configurations with three sacrificial bonds, illustrated in Fig. 4. Here, bonds A, B, and C are characterized by the dissociation energies  $D_e^{(A)} = 30 k_b T$ ,  $D_e^{(B)} = 50 k_b T$ , and  $D_e^{(C)} = 100 k_b T$ , and the maximum forces  $f_m^{(A)} = 0.21$  nN,  $f_m^{(B)} = 0.31$  nN,  $f_m^{(C)} = 0.82$  nN. The segments between the sacrificial bonds are assumed to be much stronger and therefore are not likely to break. For convenience, Fig. 5 depicts the probability of dissociation of the sacrificial bonds A, B, and C, as given by Eq. 20 with  $m = 1$ .

Fig. 4a describes a chain with internal loops that reveal a hidden length once the sacrificial bonds break. As expected, the bonds break in sequential order, based on their corresponding maximum force  $f_m$ . Note that once bonds A and B break, failure can occur through chain scission or the breaking of the interactions between the chain and the stretching device (bond

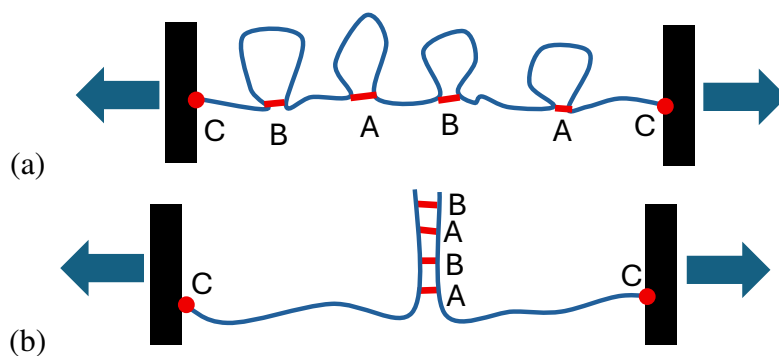


Figure 4: Several sacrificial bonds on single chains that are connected to substrates via bond C. (a) A molecule with four fixed internal loops through the sacrificial bonds A and B. Once a sufficient force is applied, a sacrificial bond breaks to reveal the corresponding hidden length from the free loop. (b) Two chain segments that are interconnected through a sequence of four sacrificial bonds (of types A and B). The application of a sufficiently large force gradually breaks the bonds to extend the length of the chain. Once all bonds dissociate, the chains break.

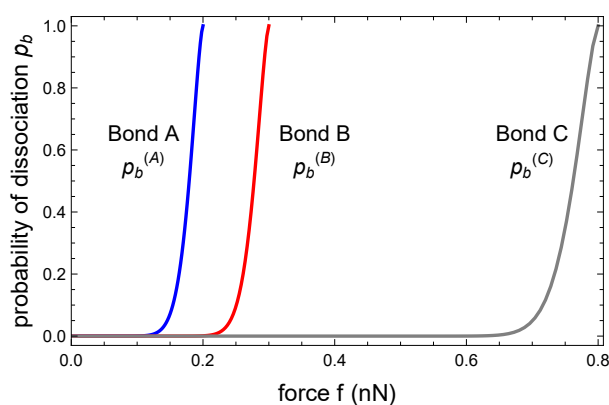


Figure 5: The probability of bond dissociation  $p_b^{(\bullet)}$  as a function of the force  $f$  for the bonds  $\bullet = A$ ,  $\bullet = B$ , and  $\bullet = C$ .

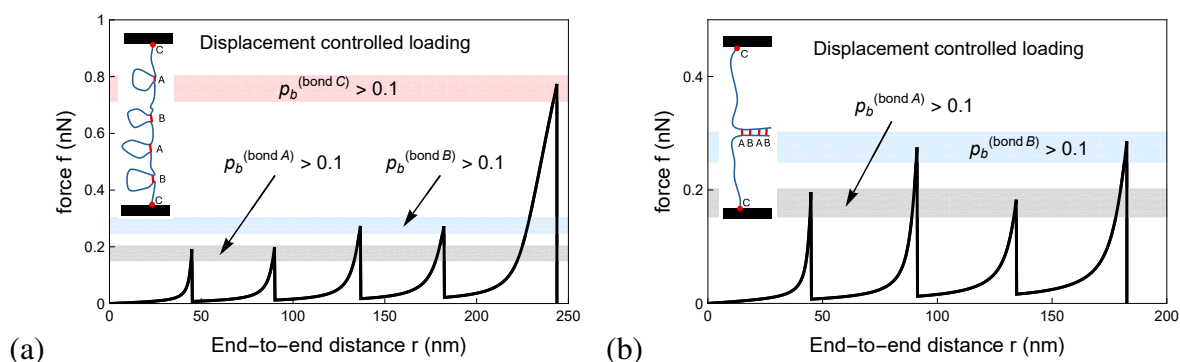


Figure 6: The force  $f$  as a function of the end-to-end distance  $r$  under displacement controlled loading for systems: (a) a molecule with four fixed internal loops through the sacrificial bonds A and B and (b) two chain segments that are interconnected through a sequence of four sacrificial bonds (of types A and B). The shaded regions denote a probability of bond dissociation  $p_b > 0.1$ .

C). Such configurations are common in single protein-based chain experiments with atomic force microscopy [67]. Since we assume that the intramolecular interactions are much stronger, detachment through the dissociation of bond C is expected to occur. Fig. 4b illustrates a chain with two parts that are interconnected by parallel bonds. Once sufficient force is applied, the bonds break successively according to the order at which they are arranged. This configuration is common in the unzipping of DNA [68, 69], where the hidden length that is released per bond dissociation is the distance between binding sites.

To demonstrate the behavior of these two systems, we consider the chains that are initially characterized by  $n = 45$  effective repeat units of length  $l_0 = 1$  nm. Each bond hides a loop segment comprising an additional 45 repeat units. Therefore, the dissociation of a bond adds 45 repeat units to the overall contour length such that the overall contour length is  $n = 45 + 45x$ , where  $x$  is the number of broken bonds.

The two systems are subjected to uniaxial extension under two types of boundary conditions: (1) displacement controlled loading and (2) force controlled loading. To determine the relation between the end-to-end distance and the applied force, we assume that the bonds experience the macroscopically applied force and calculate the probability of rupture  $p_b^{(\bullet)}$  through Eq., where  $\bullet = A, B$ , or  $C$ . Next, a random number  $0 \leq \nu \leq 1$  is generated and dissociation occurs if  $p_b^{(\bullet)} > \nu$ .

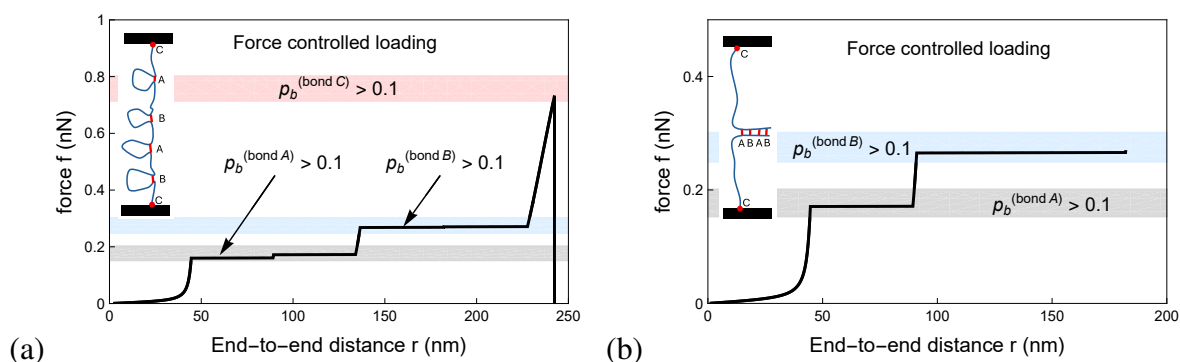


Figure 7: The force  $f$  as a function of the end-to-end distance  $r$  under force controlled loading for systems: (a) a molecule with four fixed internal loops through the sacrificial bonds A and B and (b) two chain segments that are interconnected through a sequence of four sacrificial bonds (of types A and B). The shaded regions denote a probability of bond dissociation  $p_b > 0.1$ .

Figs. 6a and 6b depict the external force  $f$  as a function of the end-to-end distance  $r$  to demonstrate the response of the two systems under displacement controlled setting (following procedure A, Sec. 2.1). The shaded regions mark a force for which  $p_b^{(\bullet)} > 0.1$ , or  $> 10\%$  bond rupture, where  $\bullet = A, B$ , or  $C$ . We point out that the relaxation of the force on the chain after a sacrificial bond breaks is proportional to the number of segments (or degrees of freedom) that are added due to the hidden length. To understand this, note that the added segments provide additional mobility that increases the entropy, and therefore decrease the applied force.

Next, we plot the force  $f$  as a function of the end-to-end distance  $r$  of the two systems under force controlled setting in Figs. 7a and 7b. Here, we follow procedure B described in Sec. 2.2. In this case, the two chains behave differently. In the case of a molecule with four fixed internal loops, once a critical force  $\sim f_m^{(A)}$  is applied, the two bonds of type A break (almost simultaneously) and a sudden “snap-through”, or an immediate extension of the chain, occurs. This effect is the result of the boundary conditions - since the force is not allowed to relax, the added repeat units from the hidden length are not allowed to relax, the entropy cannot increase, and accordingly the chain must extend abruptly to accommodate the external loading. A similar effect occurs with the two bonds of type B near the force  $\sim f_m^{(B)}$ . Further increase in loading leads to additional extension up to the force  $f_m^{(C)}$ , at which point the chain detaches.

Examination of the two chain segments that are interconnected through a sequence of four sacrificial bonds (as shown in Fig. 4b) reveals a different trend. The external force ramps up

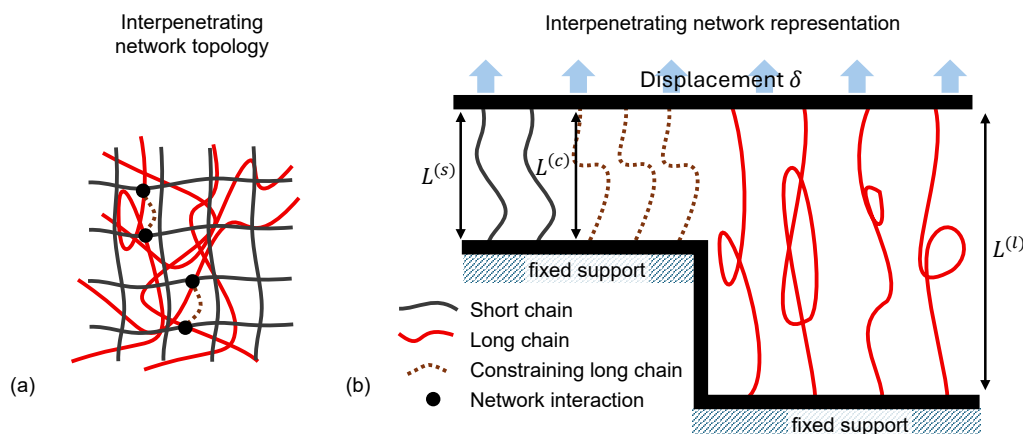


Figure 8: (a) Schematic of an interpenetrating network comprising short chains, long chains, and constraining chains that account for the network-network interactions. (b) A 1-D representation of the interpenetrating network.

to  $\sim f_m^{(A)}$ , at which point the first bond of type A dissociates and the chain instantaneously stretches. A further increase in force is required to dissociate the next bond in the sequence (bond of type B). Once the force  $\sim f_m^{(B)}$  is reached, this bond breaks. Since a monotonically increasing force is prescribed and  $f_m^{(B)} > f_m^{(A)}$ , the next two bonds immediately break as well and the chain loses its structural integrity.

The above examples emphasize the crucial role of boundary conditions in systems with sacrificial bonds - prescribing displacement allows the system to relax and regain its chain-like properties, whereas monotonic manipulation of the force leads to snap-through-like deformations and abrupt scission / detachment.

## 5 Double network polymers

To show the merit of the proposed framework, we begin by incorporating the local chain model into a simplified 1-dimensional setting to investigate double polymer networks, which are a class of interpenetrating polymer systems composed of two independently cross-linked interacting networks [53, 70]. Typically, the first network comprises short, stiff, and densely cross-linked chains, while the second network is loosely cross-linked and more extensible. The long chains in the second network often interact with the short chains through entanglements and physical

bonds [53, 54]. Henceforth, we refer to the chain segments between the interaction sites of the two networks as constraining chains (see Fig. 8a). This architectural asymmetry gives rise to a unique synergistic mechanical response that includes enhanced toughness and high strength. Broadly, under deformation the initial response is governed by the stiff network and the constraining chains. Once a sufficient load is applied, the short chains rupture and the load is transferred to the constraining chains. Additional load breaks these, resulting in a network with long chains that is characterized by high extensibility.

To understand and analyze the role of chain rupture in the mechanical response of double polymer networks, we follow the concept employed by Morovati et al. [54] and introduce a simple model and distinguish between the three families of chains, namely the short, the constraining, and the long chains. The microstructure has  $N_0 = N_0^{(s)} + N_0^{(c)} + N_0^{(l)}$  chains that are connected in parallel, where  $N_0^{(s)}$ ,  $N_0^{(c)}$ , and  $N_0^{(l)}$  denote the number of short, constraining, and long chains before damage due to chain rupture occurs, as shown in Fig. 8b. For convenience, in the following we denote quantities pertaining to short, constraining, and long chains with the superscripts  $(s)$ ,  $(c)$ , and  $(l)$ , respectively.

As a result of the network-network interactions, the short and the constraining chains are expected to have roughly the same end-to-end distance  $L^{(s)} \approx L^{(c)}$  and a comparable contour length in the undeformed state. To capture this, we define the number of repeat units  $n^{(s)} \approx n^{(c)}$ . The long chains comprise  $n^{(l)}$  repeat units and bridge the highly cross-linked domains of short and constraining chains. Therefore, these have a longer initial end-to-end distance  $L^{(l)}$ .

To simulate uniaxial extension, the chains are stretched by a displacement  $\delta$  (see Fig. 8b). The probability of chain rupture  $p_c$  increases with the displacement  $\delta$ . The total number of chains in the deformed state (at a displacement  $\delta$ ) is  $N = N^{(s)} + N^{(c)} + N^{(l)}$ , where  $N^{(\bullet)}$  denotes the number of unbroken short ( $\bullet = s$ ), constraining ( $\bullet = c$ ) and long ( $\bullet = l$ ) chains. To translate the deformation of the chains into a stress-stretch-like response, we define the macroscopic stretch as the average stretch of the three families of chains

$$\lambda = \phi^{(s)}\lambda^{(s)} + \phi^{(c)}\lambda^{(c)} + \phi^{(l)}\lambda^{(l)}, \quad (24)$$

where  $\lambda^{(\bullet)} = (L^{(\bullet)} + \delta) / L^{(\bullet)}$  is the stretch and  $\phi^{(\bullet)} = n^{(\bullet)} N^{(\bullet)} / n_t$  is the monomer fraction (or “volume” fraction) of the  $\bullet = s, c,$  or  $l$  chains. Here,  $n_t = n^{(s)} N^{(s)} + n^{(c)} N^{(c)} + n^{(l)} N^{(l)}$  is the total number of monomers in the deformed configuration. Before proceeding, we point out that (1) the deformations experienced by the chains are not affine and (2) as chains break, the total number of monomers  $n_t$  and the volume fraction of the three families of chains evolve.

Similarly, the macroscopic force required to stretch the system is given by

$$f_t = N \tilde{f}_t, \quad (25)$$

where

$$\tilde{f}_t = \frac{N^{(s)}}{N} f^{(s)} + \frac{N^{(c)}}{N} f^{(c)} + \frac{N^{(l)}}{N} f^{(l)}, \quad (26)$$

is the average force on a chain and  $f^{(\bullet)}$  is the force on the  $\bullet = s, c,$  or  $l$  chain, which is determined by solving Eq. 14 for  $\beta$  and substituting in Eq. 15.

In the following, we study two types of networks: (1) a network with no constraining chains with  $N_0^{(s)} / N_0 = 0.115$ ,  $N_0^{(c)} / N_0 = 0$ , and  $N_0^{(l)} / N_0 = 0.885$  and (2) a network characterized by  $N_0^{(s)} / N_0 = 0.1$ ,  $N_0^{(c)} / N_0 = 0.2$ , and  $N_0^{(l)} / N_0 = 0.7$ . We set the length of a repeat unit  $l_0 = 0.6$  nm and the number of repeat units in the chains as  $n^{(s)} = 6$ ,  $n^{(c)} = 6.5$ , and  $n^{(l)} = 18$ , where we note that the contour length of the long chains is three times that of the short chains. This corresponds to a ratio of long and constraining chains to short chains  $(N_0^{(c)} n^{(c)} + N_0^{(l)} n^{(l)}) / (N_0^{(s)} n^{(s)}) \sim 23$  in the undeformed configuration for both cases, which corresponds to experiments [53] and enables a fair comparison. The maximum force for the short chains is  $f_m^{(s)} = 10$  nN and, since the constraining and the long chains have the same chemical composition and are expected to be weaker than the short chains,  $f_m^{(c)} = f_m^{(l)} = 7$  nN.

To determine the conformation of the chains in the undeformed network, we first note that the stiff network is made of almost rigid short chains that are highly cross-linked. Consequently, these short chains are driven into a highly extended conformation, placing them under significant tension and “priming” them to act as sacrificial bonds that dissipate energy at low macroscopic stretches. Simultaneously, the second network of long, flexible chains is synthesized

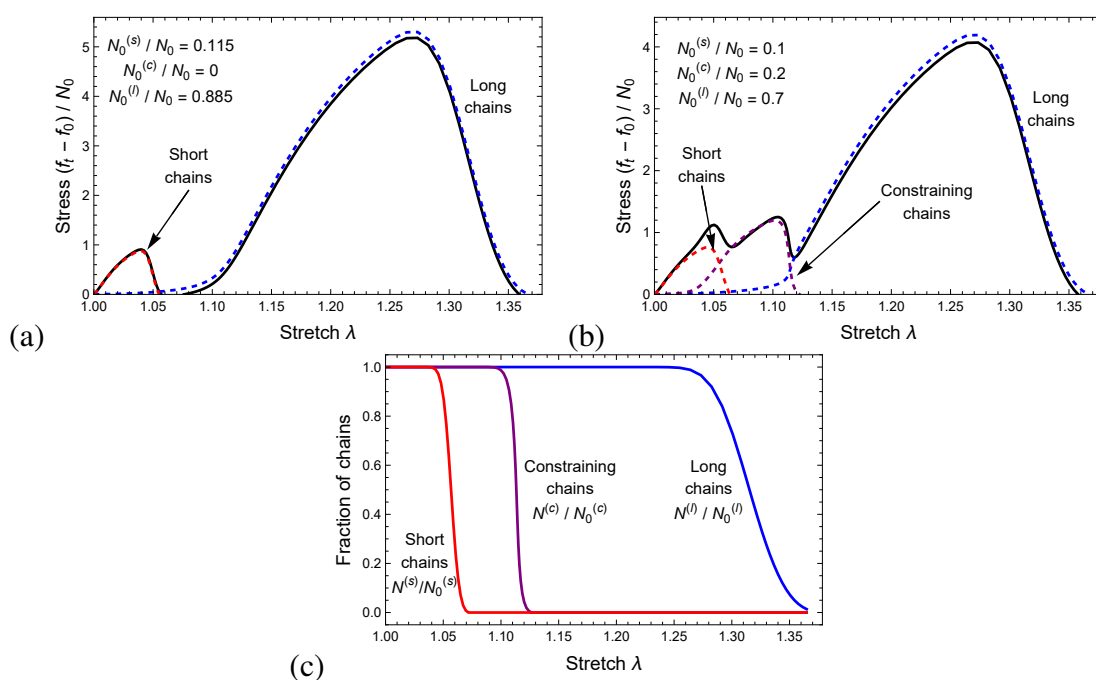


Figure 9: The stress measure  $(f_t - f_0) / N_0$  as a function of the macroscopic stretch  $\lambda$  of a double interpenetrating network with (a) short and long chains (no constraining chains) and (b) three families of chains. (c) The fraction of chains  $N^{(\bullet)} / N_0^{(\bullet)}$  as a function of the stretch  $\lambda$ .

within this dense, rigid mesh. As previously stated, the stiff network imposes severe geometric constraints on the second network of long flexible chains. This physical confinement prevents the long chains from relaxing into their thermodynamically preferred random-coil state, effectively forcing an end-to-end distance that is significantly larger than their equilibrium value. To account for these two factors, one can set the initial ratio  $\rho^{(\bullet)} = L^{(\bullet)} / n^{(\bullet)} l_0$  between the end-to-end distance  $L^{(\bullet)}$  and the initial contour length  $n^{(\bullet)} l_0$  of the short ( $\bullet = s$ ), constraining ( $\bullet = c$ ), and long ( $\bullet = l$ ) chains. Accordingly, the stiff network is assumed to be fully extended with  $\rho^{(s)} = 1$  such that any deformation of the short chains is the result of bond extension. The ratio of the constraining and the long chains is assumed to be  $\rho^{(c)} = 0.92$  and  $\rho^{(l)} = 0.9$ , respectively. It is further noted that the choice of resting length for the different families of chains in the undeformed state of the double-network polymer is non-standard, but motivated from the processes followed to synthesize the polymer, as well as from the phenomenology of the response.

The initial non-zero ratios  $\rho^{(\bullet)}$  of the three families of chains lead to a force  $f_0 > 0$  in the initial configuration of the system. A similar force appears in the classical theory of rubber

elasticity, in which chains assume an initial end-to-end distance of  $\sqrt{n}l_0$ . In a 3-dimensional network, this force leads to stress which is balanced by a scalar pressure-like term to yield zero stress in the reference configuration. In this work, we follow similar lines and define the nominal “stress” measure  $(f_t - f_0)/N_0$ , such that the reference configuration is stress free. The same definition is used to account for the “stress” on the short, the constraining, and the long chains.

Figs. 9a and 9b depict the stress  $(f_t - f_0)/N_0$  as a function of the stretch  $\lambda$  for double networks with ) short and long chains (no constraining chains) and the three families of chains, respectively. The stress of the chains are denoted by the dashed curves and the macroscopic response is the continuous black curve. As expected, the initial response is governed by the short chains. Once a sufficiently large force is applied, these chains gradually rupture. Examination of Fig. 9a shows that in the absence of constraining chains, the rupture of the short chains leads to a significant drop in stress. This stems from the transfer of load to the long and compliant long chains. However, the presence of constraining chains assists in a gradual transition of the load and therefore delays the drop in force. This leads to a plateau-like behavior, as shown in Fig. 9b. Further increase in stretch is enabled by the extension of the long chains, which provides an enhancement in the toughness.

To better understand the microstructural evolution, Fig. 9c depicts the fraction of ruptured chains  $N^{(\bullet)}/N_0^{(\bullet)}$  as a function of the stretch  $\lambda$ . It is shown that the population of the short chains begins to decrease at  $\lambda \sim 1.05$ , at which point the constraining chains take over. This can be understood by examining the dashed red and purple curves in Fig. 9b. The stretch  $\lambda \sim 1.11$  is the onset of rupture of the constraining chains, and the ultimate failure of the polymer begins at  $\lambda \sim 1.26$ .

It is important to note that the chains in real polymer networks are polydispersed. Specifically, the short, the constraining, and the long chains have a distribution of contour lengths and end-to-end distances. The polydispersity, which arises naturally during the polymerization process, forces a smooth transition of forces between the different families of chains and attenuates the drops in force seen in Figs. 9a and b. As a result, in experiments the transition between

the chains is often seen as a plateau, stemming from the integration of the local polydispersed chains from the chain to the macroscopic level.

Additionally, the simulation shows relatively low extensibility ( $\lambda \sim 1.26$ ) compared to experimental values. This is primarily because the number and length of the constraining chains are held fixed. A more realistic model — one that incorporates a distribution of constraining chain lengths in a 3-dimensional network and allows their number to evolve as damage accumulates — would produce a significantly longer and more flat yield plateau and hence extensibility.

## 6 Implementation to 3-dimensional networks

The proposed local chain model can be integrated into a 3-dimensional network to capture the macroscopic response of polymer networks and gels subjected to general loading conditions. In the following, we demonstrate this in the context of (1) a 3-dimensional network with an isotropic distribution of chains and (2) the eight-chain model of Arruda and Boyce [9]. To capture the effect of chain scission in the network, we define a coordinate system  $\{\hat{\mathbf{x}}, \hat{\mathbf{y}}, \hat{\mathbf{z}}\}$  such that the referential direction of a chain can be written as

$$\hat{\mathbf{R}}(\theta_{ch}, \phi_{ch}) = \cos \theta_{ch} \hat{\mathbf{x}} + \sin \theta_{ch} (\cos \phi_{ch} \hat{\mathbf{y}} + \sin \phi_{ch} \hat{\mathbf{z}}), \quad (27)$$

where  $0 \leq \theta_{ch} \leq \pi$  and  $0 \leq \phi_{ch} < 2\pi$  are the polar and the azimuthal angles, respectively.

Next, we define the damage parameter

$$d = \int_0^{2\pi} \int_0^\pi p_c \, d\Gamma_{ch}, \quad (28)$$

where  $d\Gamma_{ch} = (\sin \theta_{ch}/4\pi) \, d\theta_{ch} \, d\phi_{ch}$  is the normalized solid angle which accounts for the number of chains along the direction  $\hat{\mathbf{R}}(\theta_{ch}, \phi_{ch})$  and  $p_c(f)$  is the probability of breaking a chain along the direction  $\hat{\mathbf{R}}(\theta_{ch}, \phi_{ch})$  that is subjected to a force  $f$ , given in Eq. 23.

The model parameters used in the following are  $n = 10$ ,  $l_0 = 0.6 \text{ nm}$ ,  $m = 5$ ,  $f_m = 7 \text{ nN}$ , and  $D_e = 145 \, k_b T$ .

## 6.1 An isotropic network of chains

We begin by considering a network with randomly oriented and uniformly distributed chains. As before, each chain comprises  $n$  repeat units with an initial length  $l_0$ . The chain-density along the direction  $\hat{\mathbf{R}}^{(i)}$  is  $N_0^{(i)} = N_0 d\Gamma_{ch}$ , and the referential end-to-end vector of the  $i$ -th chain is  $\mathbf{R}^{(i)} = R\hat{\mathbf{R}}^{(i)}$ , where  $R = \sqrt{nl_0}$ .

The network is subjected to a macroscopic deformation characterized by the deformation gradient  $\mathbf{F}$ . We assume that the chains experience affine deformations such that the deformed end-to-end vector of the  $i$ -th chain is  $\mathbf{r}^{(i)} = \mathbf{F}\mathbf{R}^{(i)}$ . The end-to-end distance and the direction of this chain are  $r^{(i)} = \sqrt{\mathbf{r}^{(i)} \cdot \mathbf{r}^{(i)}}$  and  $\hat{\mathbf{r}}^{(i)} = \mathbf{r}^{(i)}/r^{(i)}$ . In the deformed state, the chain-density along the  $i$ -th direction is  $N^{(i)} = (1 - p_c) N_0^{(i)}$ , where  $p_c$  depends on the orientation.

The energy of the chain  $\psi_c = U_c - TS_c$  and accordingly, one can define the stress associated with the  $i$ -th chain

$$\boldsymbol{\sigma}_c^{(i)} = \frac{\partial \psi_c}{\partial \mathbf{F}} \mathbf{F}^T = k_b T n \beta (\rho^{(i)}) \rho^{(i)} \hat{\mathbf{r}} \otimes \hat{\mathbf{r}}. \quad (29)$$

The energy of the network is

$$\psi = N_0 \int_0^{2\pi} \int_0^\pi (1 - p_c) \psi_c^{(i)} d\Gamma_{ch}, \quad (30)$$

and the total true stress is

$$\boldsymbol{\sigma} = N_0 \int_0^{2\pi} \int_0^\pi (1 - p_c) \boldsymbol{\sigma}_c^{(i)} d\Gamma_{ch} - p_r \mathbf{I}. \quad (31)$$

Here,  $p_c = p_c(\theta_{ch}, \phi_{ch}, \mathbf{F})$  and  $p_r$  is the work-less pressure-like term that is determined from the boundary conditions and enforces the incompressibility of the network. The first Piola-Kirchhoff stress is  $\mathbf{P} = \boldsymbol{\sigma} \mathbf{F}^{-T}$ . We also compute the total number of chains

$$N = N_0 \int_0^{2\pi} \int_0^\pi (1 - p_c) d\Gamma_{ch}, \quad (32)$$

which can be related to the damage via  $d = 1 - N/N_0$  through Eq. 28. Here,  $N_0$  and  $N$  are the

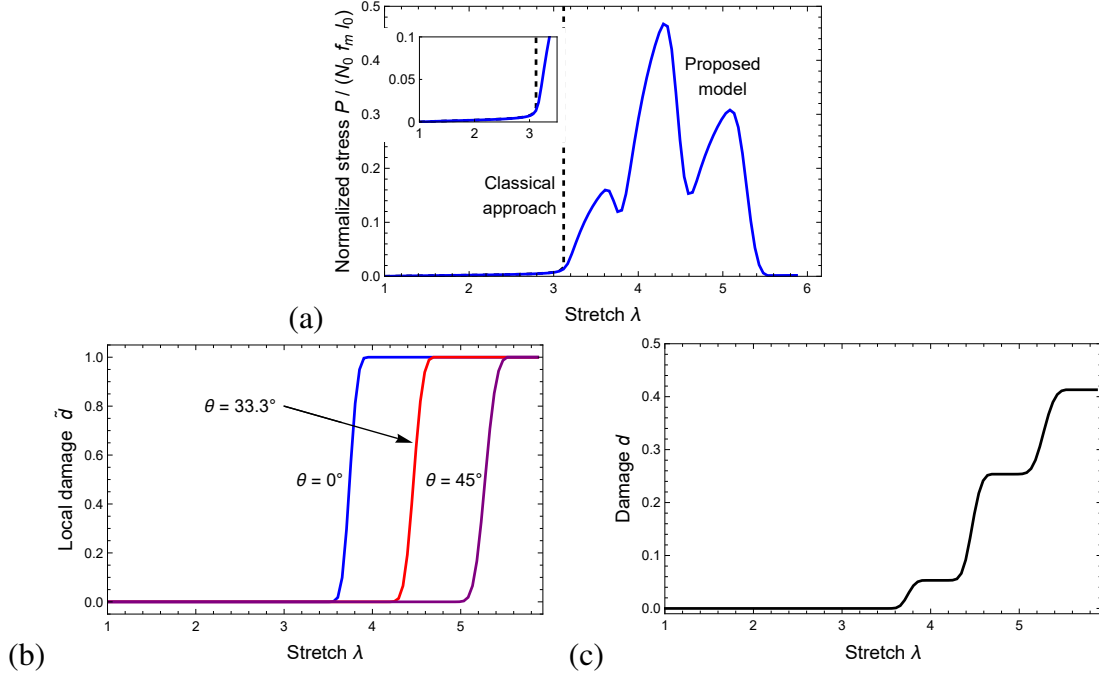


Figure 10: (a) The normalized stress  $P / (N_0 f_m l_0)$ , (b) the local damage  $\tilde{d}$ , and (c) the global damage  $d$  as a function of the uniaxial stretch  $\lambda$ .

number of chains per unit referential volume.

To demonstrate the response and damage that accumulates in a network, we focus on incompressible polymers and employ the formulations to the special case of uniaxial extension, characterized by the deformation gradient

$$\mathbf{F}_u = \lambda \hat{\mathbf{x}} \otimes \hat{\mathbf{x}} + \frac{1}{\sqrt{\lambda}} (\hat{\mathbf{y}} \otimes \hat{\mathbf{y}} + \hat{\mathbf{z}} \otimes \hat{\mathbf{z}}). \quad (33)$$

Note that under uniaxial deformation, one can rewrite  $p_c(f) = p_c(\lambda, \theta_{ch}, \phi_{ch})$ . The boundary conditions are prescribed through  $\lambda$  and the traction free boundaries  $\boldsymbol{\sigma} \hat{\mathbf{y}} \cdot \hat{\mathbf{y}} = \boldsymbol{\sigma} \hat{\mathbf{z}} \cdot \hat{\mathbf{z}} = 0$ , which enable to determine the pressure term  $p_r$ . To perform the integration from the chain to the network level, we employ the micro-sphere technique described in Appendix B with 42 representative directions (given in Table 1 of Bažant and Oh [55]).

Fig. 10a plot the normalized stress  $P / (N_0 f_m l_0)$  as a function of the stretch  $\lambda$ . Since the chains are characterized by a limiting force, the normalization  $N_0 f_m l_0 = \beta_m N_0 k_b T$ , where  $\beta_m = f_m l_0 / k_b T$  denotes the maximum value of  $\beta$  at the rupture force  $f_m$ , is used for convenient.

The dashed curve corresponds to the response according to the classical theory, where  $\beta$  is determined from the Langevin function, and the continuous curve is the proposed model.

To demonstrate the progressive damage in the network, we note that the response of chains is symmetric with respect to the stretching direction  $\hat{\mathbf{x}}$  and therefore define the local damage of chains characterized by an angle  $\theta_{ch}$  via  $\tilde{d}(\lambda, \theta_{ch}) = \int_0^{2\pi} p_c(\lambda, \theta_{ch}, \phi_{ch}) / 2\pi d\phi_{ch}$ . Fig. 10b plots the local damage  $\tilde{d}$  of a family of chains that form the an angle  $\theta_{ch}$  with respect to the stretching direction  $\hat{\mathbf{x}}$ . We select the three representative angles  $\theta_{ch} = 0^\circ, 33.3^\circ$ , and  $45^\circ$ , which characterize the representative directions in the chosen micro-sphere integration scheme. The total damage  $d$ , as defined in Eq. 28, is depicted in 10c.

As expected, the proposed model exhibits the same response as the classical approaches under small-to-moderate deformations. However, as the chains stretch close to their contour length, the stress approaches its limit and rupture begins. First, chain scission occurs in chains that are aligned along the stretching direction. As further stretch is applied, more chains rotate towards the  $\hat{\mathbf{x}}$ -direction and elongate, leading to the ultimate failure of the network. It is worth noting that the gradual scission events are characterized by a local drop in stress (or the “humps”) in Fig. 10a and as “steps” in the damage curve shown in 10c. However, it is underscored that the micro-sphere-based integration employed in this work employs 42 representative directions, characterized by 5 angles  $\theta_{ch}$  (see Table 1 in Bažant and Oh [55]). As shown by Mulderrig et al. [25], consideration of additional chain orientations through higher quadrature schemes is expected to lead to a smoother transition in the stress-stretch and the damage-stretch curves at additional computational cost.

## 6.2 The eight-chain model

The previous framework, which accounts for the different chain orientations in the network, is advantageous since it can capture the gradual rupture of chains and provides a more robust realization of the network. However, its main drawback is the high computational cost required to obtain a solution, which increases dramatically as more chain orientations are considered [25]. To overcome this, we also propose to embed the local chain response into the eight-chain

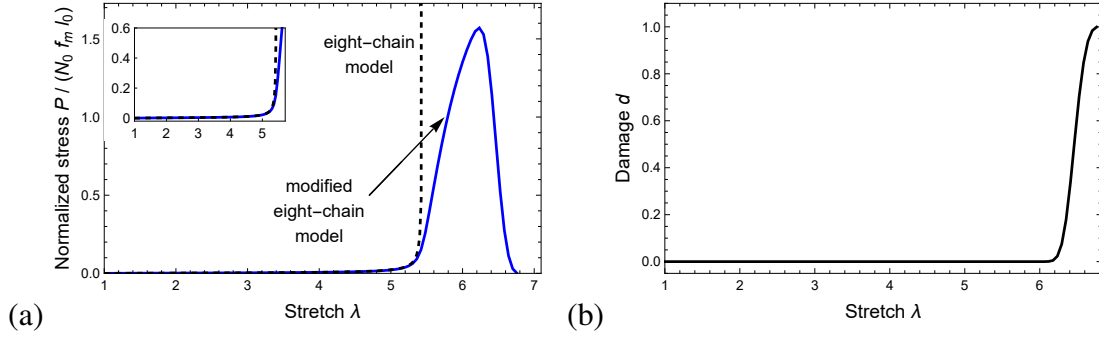


Figure 11: (a) The normalized stress  $P / (N_0 f_m l_0)$  and (b) the damage  $d$  as a function of the uniaxial stretch  $\lambda$  for a polymer subjected to uniaxial stretch.

topology proposed by Arruda and Boyce [9]. Broadly, this model assumes that the response of an incompressible network with  $N_0$  referential chains per unit volume, where each chain comprises  $n$  repeat units of an initial length  $l_0$ , can be determined from eight representative chains that describe the underlying structure.

The network is subjected to a deformation gradient  $\mathbf{F}$  and, in a deformed state, is has  $N = (1 - d) N_0$  (the damage parameter  $d$  is given in Eq. 28). The stretch of the eight chains is  $\lambda_c = r/R = \sqrt{I_1/3}$ , where  $I_1 = \text{Tr}(\mathbf{F}^T \mathbf{F})$  is the first invariant. Subsequently, the free energy of a chain  $\psi_c = U_c - TS_c$  can be computed and the total strain energy-density is  $\psi = N\psi_c$ . The true stress tensor is then

$$\boldsymbol{\sigma} = Nk_b T \beta \sqrt{\frac{n}{3I_1}} \mathbf{F} \mathbf{F}^T - p_r \mathbf{I}, \quad (34)$$

where, as before,  $p_r$  is the pressure term that enforces incompressibility and is determined from the boundary conditions. Recall that  $\beta$  is determined from Eq. 14. Once again, we recall that the first Piola-Kirchhoff stress tensor  $\mathbf{P} = \boldsymbol{\sigma} \mathbf{F}^{-T}$ .

It is emphasized that since the response of the network is based on the assumption that the eight representative chains experience the same deformation  $\lambda_c = \sqrt{I_1/3}$  [9], the damage in Eq. 28 simplifies to  $d = p_c$ .

To demonstrate the response and the damage in the network, we consider a polymer subjected to uniaxial extension characterized by the deformation gradient  $\mathbf{F}_u$  (Eq. 33). By employing the boundary conditions  $\boldsymbol{\sigma} \hat{\mathbf{y}} \cdot \hat{\mathbf{y}} = \boldsymbol{\sigma} \hat{\mathbf{z}} \cdot \hat{\mathbf{z}} = 0$ , one can determine the pressure term and the

uniaxial nominal stress

$$P = Nk_bT\beta\sqrt{\frac{n}{3I_1}}\left(\lambda - \frac{1}{\lambda^2}\right). \quad (35)$$

Figs. 11a and 11b plot the normalized stress  $P/(N_0f_ml_0)$  (Eq. 35) and the damage  $d = p_c$  (Eq. 28) as a function of the stretch  $\lambda$  for a polymer network. Since the chains are characterized by a limiting force, the normalization  $N_0f_ml_0 = \beta_m N_0k_bT$ , where  $\beta_m = f_ml_0/k_bT$  denotes the maximum value of  $\beta$  at the rupture force  $f_m$ , is used for convenience. The proposed model recovers the classical eight-chain under small to moderate stretches. However, at large deformations the proposed model captures the extensibility of the repeat units, chain scission, and the reduction in chains. Examination of the damage in 11b shows that at a stretch  $\lambda \sim 6.2$  chains begin to rupture and the network fails.

## 7 Conclusions

This contribution investigates the origin of failure in polymer chains. To this end, we consider FJCs with extensible segments to account for the entropic and the enthalpic energies that are stored in a chain that is subjected to stretching. As opposed to other works, which consider a variation in the stretching of the Kuhn segments through the partition function, the proposed framework computes the Kuhn length directly through the maximization of the entropy. The model reveals that the external force applied to a chain is unequally distributed along the repeat units. Specifically, segments that are aligned along the end-to-end direction experience the maximum force. This allows to compute the local probability of bond rupture, which is the highest in repeat units that are aligned along the end-to-end vector. In turn, one can determine the probability of chain scission.

To capture the enthalpic contribution, a tilted Morse-potential is employed to the Kuhn segments. Following previous works, we assume that the probability of rupture of bonds along a Kuhn segment depend on the activation energy. In the absence of a mechanical force, this energy is high (on the order of  $150 k_bT$ ) and therefore bond rupture is highly unlikely. The application of an external force shifts the energy landscape, and consequently two extrema points are obtained along the potential energy - a minimum that describes the equilibrium state

and a maximum that characterizes the transition state. The activation energy, which is defined as the difference between these two energies, decreases with the applied force and accordingly the probability of a rupture event increases. Once the activation energy is zero, bond dissociation occurs spontaneously. Chain scission occurs once one of the bonds break, and accordingly the probability of failure can be computed.

To demonstrate the merit of the framework, we examine the response of chains with stiff C-C bonds and compliant physical bonds. The latter is of particular interest to networks with sacrificial bonds or mechanophores, in which weaker bonds can rupture prior to the main chain, interpenetrating networks comprising two or more families of chains, where the failure of specific chains activates other chains and provide a network with enhanced toughness, and biological polymers in which various potential failure mechanisms can be triggered. In the case of double networks, we combined our single-chain model with a non-affine framework that accounts for interactions between the stiff and soft networks to reproduce the necking plateau observed experimentally through a simplified 1-dimensional setting. To enable predictive capabilities under a general loading, we also show that the local chain model can be integrated to continuum-level model representation of 3-dimensional networks using the numerical micro-sphere method as well as the well-known eight chain model.

This work provides a physically-based model to quantify the stretching and failure of a single chain and can be used to develop coarse grain description of damage in polymer networks.

## Appendix

### A Derivation of the force on a chain

To derive the stretching force  $f$ , we first write

$$U_c - TS_c = k_b T \left( -n \ln n + \alpha n + \frac{\beta}{l_0} r \right), \quad (36)$$

where the relation  $\gamma = -1/k_bT$  is employed. Note that  $\alpha = \alpha(r)$  and  $\beta = \beta(r)$ , and therefore

$$\frac{\partial (U_c - TS_c)}{\partial r} = k_bT \left( n \frac{\partial \alpha}{\partial r} + \frac{r}{l_0} \frac{\partial \beta}{\partial r} \right) + \frac{k_bT}{l_0} \beta. \quad (37)$$

We continue by calculating the derivatives. The Lagrange multiplier is  $\alpha = \ln(n/Z)$  and its derivative is

$$\frac{\partial \alpha}{\partial r} = -\frac{1}{Z} \frac{\partial Z}{\partial \beta} \frac{\partial \beta}{\partial r}. \quad (38)$$

Substitution of Eq. 38 into Eq. 37 yields

$$\frac{\partial (U_c - TS_c)}{\partial r} = k_bT \left( -\frac{n}{Z} \frac{\partial Z}{\partial \beta} + \frac{r}{l_0} \right) \frac{\partial \beta}{\partial r} + \frac{k_bT}{l_0} \beta. \quad (39)$$

The derivative of the partition function is determined from Eq. 11 in the main manuscript,

$$\begin{aligned} \frac{n}{Z} \frac{\partial Z}{\partial \beta} &= n \int_0^\pi \left( \frac{l}{l_0} \cos \theta + \left( \beta \frac{\cos \theta}{l_0} - \frac{1}{k_bT} \frac{\partial u}{\partial l} \right) \frac{\partial l}{\partial \beta} \right) p_\theta d\Gamma \\ &= n \int_0^\pi \frac{l}{l_0} \cos \theta p_\theta d\Gamma = \frac{r}{l_0}, \end{aligned} \quad (40)$$

where we employ the relation  $\partial u / \partial l = k_bT \beta \cos \theta / l_0$  (Eq. 7) and Eq. 13 in the main manuscript in passing.

Finally, substitution of Eq. 40 into Eq. 39 yields

$$f = \frac{\partial (U_c - TS_c)}{\partial r} = \frac{k_bT}{l_0} \beta. \quad (41)$$

## B The micro-sphere technique

To integrate from the chain to the network level, we employ the micro-sphere technique proposed by Bažant and Oh [55]. This method was later used to capture the response on rubbery networks [56, 71].

Consider a unit sphere with a surface that represents the end-to-end directions of the chains.

The directional averaging of a quantity  $\bullet$  can be approximated through the discrete summation

$$\langle \bullet \rangle = \frac{1}{4\pi} \int_A \bullet \, dA = \sum_{i=1}^m \bullet^{(i)} w^{(i)}, \quad (42)$$

where  $i = 1, \dots, m$  are the representative chain directions  $\hat{\mathbf{R}}^{(i)}$ ,  $\bullet^{(i)}$  is the value of the variable being averaged along the  $i$ -th direction, and  $w^{(i)}$  are appropriate non-negative weights, constrained by  $\sum_{i=1}^m w^{(i)} = 1$ .

In the special case of randomly oriented and uniformly distributed networks, one requires  $\sum_{i=1}^m \hat{\mathbf{R}}^{(i)} w^{(i)} = \mathbf{0}$  and  $\sum_{i=1}^m \hat{\mathbf{R}}^{(i)} \otimes \hat{\mathbf{R}}^{(i)} w^{(i)} = 1/3\mathbf{I}$ .

Bažant and Oh [55] showed that a specific choice of  $m = 42$  representative directions provide sufficient accuracy for isotropically distributed directions. In this work, we follow this conclusion. The integration directions and the corresponding weight function are given in Table 1 of Bažant and Oh [55].

## References

- [1] Ghatak, A., Vorvolakos, K., She, H., Malotky, D. L., and Chaudhury, M. K. (2000) Interfacial Rate Processes in Adhesion and Friction. *J. Phys. Chem. B* 104, 4018–4030.
- [2] Lavoie, S. R., Long, R., and Tang, T. (2016) A rate-dependent damage model for elastomers at large strain. *Extreme Mechanics Letters* 8, 114–124.
- [3] Mao, Y., Talamini, B., and Anand, L. (2017) Rupture of polymers by chain scission. *Extreme Mechanics Letters* 13, 17–24.
- [4] Lamont, S. C., Mulderrig, J., Bouklas, N., and Vernerey, F. J. (2021) Rate-Dependent Damage Mechanics of Polymer Networks with Reversible Bonds. *Macromolecules* 54, 10801–10813.
- [5] Lamont, S. C., Bouklas, N., and Vernerey, F. J. (2025) Cohesive instability in elastomers: insights from a crosslinked Van der Waals fluid model. *International Journal of Fracture* 249, 20.

- 
- [6] Wang, S.-Q., Fan, Z., Siavoshani, A., Wang, M.-c., and Wang, J. (2025) Fresh considerations regarding time-dependent elastomeric fracture. *Extreme Mechanics Letters* 74, 102277.
- [7] Wang, M. C., and Guth, E. (1952) Statistical Theory of Networks of Non-Gaussian Flexible Chains. *J. Chem. Phys.* 20, 1144–1157.
- [8] Treloar, L. R. G. (1946) The elasticity of a network of long-chain molecules.–III. *Trans. Faraday Soc.* 42, 83–94.
- [9] Arruda, E. M., and Boyce, M. C. (1993) A three-dimensional constitutive model for the large stretch behavior of rubber elastic materials. *Journal of the Mechanics and Physics of Solids* 41, 389–412.
- [10] Kuhn, W., and Grun, F. (1942) Beziehungen zwischen elastischen Konstanten und Dehnungsdoppelbrechung hochelastischer Stoffe. *Kolloid-Zeitschrift* 101, 248–271.
- [11] Zhu, J., and Brassart, L. (2025) Stretching Response of a Polymer Chain with Deformable Bonds. *PRL* 134, 218101.
- [12] Webber, R. E., Creton, C., Brown, H. R., and Gong, J. P. (2007) Large Strain Hysteresis and Mullins Effect of Tough Double-Network Hydrogels. *Macromolecules* 40, 2919–2927.
- [13] Wang, X., and Hong, W. (2011) Pseudo-elasticity of a double network gel. *Soft Matter* 7, 8576–8581.
- [14] Brown, H. R., Hui, C. Y., and Raphael, E. (1994) Interplay between intermolecular interactions and chain pullout in the adhesion of elastomer. *Macromolecules* 27, 608–609.
- [15] Creton, C., Kramer, E. J., Brown, H. R., and Hui, C.-Y. *Molecular Simulation Fracture Gel Theory*; Springer Berlin Heidelberg: Berlin, Heidelberg, 2002; pp 53–136.

- 
- [16] Lavoie, S. R., Millereau, P., Creton, C., Long, R., and Tang, T. (2019) A continuum model for progressive damage in tough multinetwork elastomers. *Journal of the Mechanics and Physics of Solids* 125, 523–549.
- [17] Yang, T., Liechti, K. M., and Huang, R. (2020) A multiscale cohesive zone model for rate-dependent fracture of interfaces. *Journal of the Mechanics and Physics of Solids* 145, 104142.
- [18] Lake, G. J., and Thomas, A. G. (1967) The strength of highly elastic materials. *Proc. A* 300, 108–119.
- [19] Li, X., and Gong, J. P. (2024) Design principles for strong and tough hydrogels. *Nature Reviews Materials* 9, 380–398.
- [20] Ducrot, E., Chen, Y., Bulters, M., Sijbesma, R. P., and Creton, C. (2014) Toughening Elastomers with Sacrificial Bonds and Watching Them Break. *Science* 344, 186–189.
- [21] Sloopman, J., Waltz, V., Yeh, C. J., Baumann, C., Göstl, R., Comtet, J., and Creton, C. (2020) Quantifying Rate- and Temperature-Dependent Molecular Damage in Elastomer Fracture. *Phys. Rev. X* 10, 041045.
- [22] Vernerey, F. J., Brighenti, R., Long, R., and Shen, T. (2018) Statistical damage mechanics of polymer networks. *Macromolecules* 51, 6609–6622.
- [23] Itskov, M., and Knyazeva, A. (2016) A rubber elasticity and softening model based on chain length statistics. *International Journal of Solids and Structures* 80, 512–519.
- [24] Itskov, M., and Darabi, E. (2016) Constitutive modeling of carbon nanotube rubber composites on the basis of chain length statistics. *Composites Part B: Engineering* 90, 69–75.
- [25] Mulderrig, J., Li, B., and Bouklas, N. (2021) Affine and non-affine microsphere models for chain scission in polydisperse elastomer networks. *Mechanics of Materials* 160, 103857.
- [26] Volokh, K. Y. (2010) On modeling failure of rubber-like materials. *Mechanics Research Communications* 37, 684–689.

- 
- [27] Volokh, K. Y. (2013) Review of the energy limiters approach to modeling failure of rubber. *Rubber Chemistry and Technology* 86, 470–487.
- [28] Mulderrig, J., Talamini, B., and Bouklas, N. (2023) A statistical mechanics framework for polymer chain scission, based on the concepts of distorted bond potential and asymptotic matching. *Journal of the Mechanics and Physics of Solids* 174, 105244.
- [29] Buche, M. R., Silberstein, M. N., and Grutzik, S. J. (2022) Freely jointed chain models with extensible links. *PRE* 106, 024502.
- [30] Buche, M. R., and Silberstein, M. N. (2020) Statistical mechanical constitutive theory of polymer networks: The inextricable links between distribution, behavior, and ensemble. *PRE* 102, 012501.
- [31] Buche, M. R., and Silberstein, M. N. (2021) Chain breaking in the statistical mechanical constitutive theory of polymer networks. *Journal of the Mechanics and Physics of Solids* 156, 104593.
- [32] Olive, R., and Cohen, N. (2024) Deformation and failure mechanisms in spider silk fibers. *Journal of the Mechanics and Physics of Solids* 182, 105480.
- [33] Hillgartner, M., Linka, K., and Itskov, M. (2018) Worm-like chain model extensions for highly stretched tropocollagen molecules. *Journal of Biomechanics* 80, 129–135.
- [34] Cohen, N., and Zhang, F. (2025) Modeling of protein networks reveals factors affecting stiffness, yield stress, and strain stiffening in silk fibers. *Acta Biomaterialia* 208, 402–410.
- [35] Du, N., Yang, Z., Liu, X. Y., Li, Y., and Xu, H. Y. (2011) Structural Origin of the Strain-Hardening of Spider Silk. *Adv. Funct. Mater.* 21, 772–778.
- [36] Qian, J., Lin, J., Xu, G.-K., Lin, Y., and Gao, H. (2017) Thermally assisted peeling of an elastic strip in adhesion with a substrate via molecular bonds. *Journal of the Mechanics and Physics of Solids* 101, 197–208.

- 
- [37] Keren, S., Segal-Peretz, T., and Cohen, N. (2023) Exploiting perforations to enhance the adhesion of 3D-printed lap shears. *Theoretical and Applied Fracture Mechanics* 126, 103986.
- [38] Zhang, W., Zou, S., Wang, C., and Zhang, X. (2000) Single polymer chain elongation of poly (N-isopropylacrylamide) and poly (acrylamide) by atomic force microscopy. *The Journal of Physical Chemistry B* 104, 10258–10264.
- [39] Zhang, W., and Zhang, X. (2003) Single molecule mechanochemistry of macromolecules. *Progress in Polymer Science* 28, 1271–1295.
- [40] Beyer, M. K. (2000) The mechanical strength of a covalent bond calculated by density functional theory. *J. Chem. Phys.* 112, 7307–7312.
- [41] Wang, S., Panyukov, S., Rubinstein, M., and Craig, S. L. (2019) Quantitative Adjustment to the Molecular Energy Parameter in the Lake-Thomas Theory of Polymer Fracture Energy. *Macromolecules* 52, 2772–2777.
- [42] Miehe, C., and Schanzel, L.-M. (2014) Phase field modeling of fracture in rubbery polymers. Part I: Finite elasticity coupled with brittle failure. *Journal of the Mechanics and Physics of Solids* 65, 93–113.
- [43] Ang, I., Bouklas, N., and Li, B. (2022) Stabilized formulation for phase-field fracture in nearly incompressible hyperelasticity. *Int J Numer Methods Eng* 123, 4655–4673.
- [44] Peerlings, R. H. J., De Borst, R., Brekelmans, W. A. M., and De Vree, J. H. P. (1996) Gradient enhanced damage for quasi-brittle materials. *Int. J. Numer. Meth. Engng.* 39, 3391–3403.
- [45] Mousavi, S. M., Ang, I., Mulderrig, J., and Bouklas, N. (2024) Evaluating Fracture Energy Predictions Using Phase-Field and Gradient-Enhanced Damage Models for Elastomers. *J. Appl. Mech* 91.

- 
- [46] Talamini, B., Mao, Y., and Anand, L. (2018) Progressive damage and rupture in polymers. *Journal of the Mechanics and Physics of Solids* 111, 434–457.
- [47] Mousavi, S. M., Mulderrig, J., Talamini, B., and Bouklas, N. (2025) A chain stretch-based gradient-enhanced model for damage and fracture in elastomers. *Computer Methods in Applied Mechanics and Engineering* 444, 118103.
- [48] Mousavi, S. M., Mulderrig, J., Talamini, B., and Bouklas, N. (2026) Capturing the fractocohesive length scale in elastomers through a statistical mechanics-based gradient enhanced damage model. *Journal of the Mechanics and Physics of Solids* 209, 106504.
- [49] Kauzmann, W., and Eyring, H. (1940) The Viscous Flow of Large Molecules. *J. Am. Chem. Soc.* 62, 3113–3125.
- [50] Evans, E., and Ritchie, K. (1997) Dynamic strength of molecular adhesion bonds. *Biophysical Journal* 72, 1541–1555.
- [51] Fantner, G. E., Oroudjev, E., Schitter, G., Golde, L. S., Thurner, P., Finch, M. M., Turner, P., Gutsman, T., Morse, D. E., Hansma, H., and Hansma, P. K. (2006) Sacrificial Bonds and Hidden Length: Unraveling Molecular Mesostructures in Tough Materials. *Biophysical Journal* 90, 1411–1418.
- [52] Na, Y.-H., Tanaka, Y., Kawauchi, Y., Furukawa, H., Sumiyoshi, T., Gong, J. P., and Osada, Y. (2006) Necking Phenomenon of Double-Network Gels. *Macromolecules* 39, 4641–4645.
- [53] Gong, J. P. (2010) Why are double network hydrogels so tough? *Soft Matter* 6, 2583–2590.
- [54] Morovati, V., Saadat, M. A., and Dargazany, R. (2020) Necking of double-network gels: Constitutive modeling with microstructural insight. *Phys. Rev. E* 102, 062501.
- [55] Bažant, P., and Oh, B. (1986) Efficient numerical integration on the surface of a sphere.

---

*ZAMM-Journal of Applied Mathematics and Mechanics/Zeitschrift für Angewandte Mathematik und Mechanik* 66, 37–49.

- [56] Miehe, C., Göktepe, S., and Lulei, F. (2004) A micro-macro approach to rubber-like materials-part I: the non-affine micro-sphere model of rubber elasticity. *Journal of the Mechanics and Physics of Solids* 52, 2617–2660.
- [57] Flory, P. J. *Principles of polymer chemistry*; Cornell university press, 1953.
- [58] Treloar, L. G. (1975) *The physics of rubber elasticity*.
- [59] Wang, C., Shi, W., Zhang, W., Zhang, X., Katsumoto, Y., and Ozaki, Y. (2002) Force Spectroscopy Study on Poly(acrylamide) Derivatives: Effects of Substitutes and Buffers on Single-Chain Elasticity. *Nano Lett.* 2, 1169–1172.
- [60] Smith, S. B., Cui, Y., and Bustamante, C. (1996) Overstretching B-DNA: The Elastic Response of Individual Double-Stranded and Single-Stranded DNA Molecules. *Science* 271, 795–799.
- [61] Sheu, S.-Y., Yang, D.-Y., Selzle, H. L., and Schlag, E. W. (2003) Energetics of hydrogen bonds in peptides. *Proceedings of the National Academy of Sciences* 100, 12683–12687.
- [62] Zhang, H., and Diesendruck, C. E. (2023) Off-center Mechanophore Activation in Block Copolymers. *Angew. Chem. Int. Ed.* 62, e202213980.
- [63] Cohen, N. (2019) Programming the equilibrium swelling response of heterogeneous polymeric gels. *International Journal of Solids and Structures* 178-179, 81–90.
- [64] Cohen, N., Du, C., and Wu, Z. L. (2021) Understanding the Dissociation of Hydrogen Bond Based Cross-Links In Hydrogels Due to Hydration and Mechanical Forces. *Macromolecules* 10.1021/acs.macromol.1c01927.
- [65] Chen, H., Li, J., Ding, Y., Zhang, G., Zhang, Q., and Wu, C. (2005) Folding and unfolding of individual PNIPAM-g-PEO copolymer chains in dilute aqueous solutions. *Macromolecules* 38, 4403–4408.

- [66] Olive, R., and Cohen, N. (2025) Employing spinning conditions to control the mechanical response of spider silk fibers. *International Journal of Solids and Structures* 322, 113592.
- [67] Li, H., Oberhauser, A. F., Fowler, S. B., Clarke, J., and Fernandez, J. M. (2000) Atomic force microscopy reveals the mechanical design of a modular protein. *Proceedings of the National Academy of Sciences* 97, 6527–6531.
- [68] Krautbauer, R., Rief, M., and Gaub, H. E. (2003) Unzipping DNA Oligomers. *Nano Lett.* 3, 493–496.
- [69] Bockelmann, U., Thomen, P., Essevaz-Roulet, B., Viasnoff, V., and Heslot, F. (2002) Unzipping DNA with Optical Tweezers: High Sequence Sensitivity and Force Flips. *Biophysical Journal* 82, 1537–1553.
- [70] Gong, J. P., Katsuyama, Y., Kurokawa, T., and Osada, Y. (2003) Double-Network Hydrogels with Extremely High Mechanical Strength. *Adv. Mater.* 15, 1155–1158.
- [71] Cohen, N., and McMeeking, R. M. (2019) On the swelling induced microstructural evolution of polymer networks in gels. *Journal of the Mechanics and Physics of Solids* 125, 666–680.